Indian Journal of Radio & Space Physics
Vol. 43, June 2014, pp 197-204

Study of solar flare induced D-region ionosphere changes using VLF amplitude observations at a low latitude site

L M Tan[1,$,*], N N Thu[2], T Q Ha[3] & M Marbouti[4]

[1]Faculty of Natural Science and Technology, Tay Nguyen University, 567- Le Duan, Buon Ma Thuot City, Dak Lak Province 632025, Vietnam

[2]Geophysical Center, South Vietnam Geological Mapping Division, 16/9 Ky Dong, Ward 9, District 3, Ho Chi Minh City 722923, Vietnam

[3]Ho Chi Minh City University of Education, 280-An Duong Vuong, Ward 4, District 5, Ho Chi Minh City 748342, Vietnam

[4]Energy Engineering and Physics Department, Amirkabir University of Technology, 15875-4413, 424 Hafez Ave, Tehran, Iran

[$]E-mail: tantaynguyen82@yahoo.com

Received 13 March 2014; revised received and accepted 29 May 2014

About 26 solar flare events from C2.56 to X3.2 classes were obtained and analyzed at Tay Nguyen University, Vietnam (12.56°N, 108.02°E) during May – December 2013 using very low frequency remote sensing to understand the responses of low latitude D-region ionosphere during solar flares. The observed VLF amplitude perturbations are used as the input parameters for the simulated Long Wavelength Propagation Capability (LWPC) program, using Wait's model of lower ionosphere, to calculate two Wait's parameters, viz. the reflection height (*H'*) and the sharpness factor (β). The results reveal that when X-ray irradiance is increased, β increased from 0.3 to 0.506 km^{-1}, while *H'* decreased from 74 to 60 km. The electron density increased at the height of 74 km with 1-3 orders of magnitude during solar flares. These phenomena can be explained as: the ionization due to X-ray irradiance becomes greater than that due to cosmic rays and Lyman-α radiation, which increases the electron density profile. The present results are in agreement with the earlier results. The 3D representation of the electron density changes with altitude and time supports to fully understand the shape of the electron density changes due to X-ray flares. The shape variation of electron density is roughly followed to the variation of the amplitude perturbation and keeps this rule for different altitudes. It is also found that the electron density versus the height in lower latitude D-region ionosphere increases more rapidly during solar flares.

Keywords: D-region ionosphere, Solar flare, VLF amplitude perturbations, Electron density profile, Reflection height, X-ray irradiance, Sharpness factor

PACS Nos: *96.60qe*; *94.20 de*; *94.20.wq*

1 Introduction

The Earth's ionosphere is the top of the atmosphere with an altitude of 60 to 1500 km[1]. The solar radiation ionizes the gas molecules such as nitrogen (N_2) and oxygen (O_2) into positive ions and free electrons[2]. The free electrons generated by the ionization of the ionosphere can greatly affect the transmission of radio signals[3]. In the D-region (60 - 90 km), the lowest layer of the ionosphere, the level of ionization depends on the solar zenith angle and solar radiation by Chapman's theory[2]. As the sun rises, the appearance of solar electromagnetic radiation rapidly ionizes the ionosphere. Conversely, when the sun goes down, the disappearance of the electromagnetic radiation causes the decrease of ionosphere's ion density[4]. The recording of very low frequency (VLF) (3 – 30 kHz) signal transmission via ionosphere of the Earth is powerful to study the effects of solar flares on ionospheric VLF radio wave propagation[5]. In daytime, the change of the VLF strength is smooth with a maximum at mid-day. At the night, the reflection of VLF signals occurs from E-region at a height of 90 km (Ref. 6). The signal minima occurred during the path of sunrise and sunset transition due to modal interference[7].When the solar flares appear, the strong ionizing radiation takes the electron density of the D-region to dramatically increase with 1-2 orders of magnitude[8]. Therefore, the expression of the VLF receiver's records is the sudden changes of signal amplitude and phase of the VLF signals and their subsequent recovery period returning to the normal levels of the signals[9].

The X-ray flux emitted by Sun becomes the main ionization source of the D-region ionosphere. The X-ray wavelengths, which are smaller than 1 nm, affect the ionization rate of O_2 and N_2 leading to increase in the electron density[10]. The change of the

electron density with altitude is identified according to the formulation of Wait[11] and Thomson[12] models.

$$N_e(z,H',\beta) = 1.43\times10^{13}\exp(-0.15H')\times\exp\left[(\beta-0.15)(z-H')\right] \quad \ldots (1)$$

where, N_e, is the electron density (m^{-3}); z, the altitude (km); H', the reflection height; and β, the exponential sharpness factor (km^{-1}).

In the present study, the VLF signal amplitude of the NWC (North West Cape) transmitter (19.8 kHz) propagating in the Earth – Ionosphere waveguide is recorded with a distance of 3886 km from Australia (21.8°S, 114.2°E) to the VLF receiver located at Tay Nguyen University (TNU), Vietnam (12.56°N, 108.02°E). The positive VLF amplitude perturbations (in dB) were continuously observed from May – December, 2013. The Long Wavelength Propagation Capability (LWPC) code is used to calculate two parameters (H', β). Then, the changes of these parameters versus the intensity of X-ray irradiance are discussed, in addition to the electron density profile changes of D-region ionosphere during solar flares. These results are compared with the results of Basak & Chakrabarti[13] and Grubor *et al.*[8] at different latitudes to deeply comprehend the changes of this region occurred by solar flares.

2 Instrumentation and Data analysis

The VLF receiver is installed as per the standard of Ultra-MSK system[14]. This narrow-band VLF receiver includes a VLF antenna, a pre-amplifier, a sound card, a GPS receiver, a computer and Ultra-MSK software package (Fig. 1). The VLF antenna records the magnetic field component of the VLF waves. The pre-amplifier receives the weak VLF signals and filters the noises. The VLF signal is transmitted by the coaxial cable with the length of 200 m to the computer and is connected by an isolated transformer before connecting to the computer. The sound card is the M-Audio Delta 44 type, which has the sampling rate of 96 kS s^{-1} and the analog to digital conversion with a resolution of 24 bits. The GPS receiver provides 1 pulse per second (1PPS) for the sound card and Ultra-MSK software to record the data for every second. The computer has the Linux operating system. The present system uses a Butterworth low-pass filter to remove the high frequency noises. After reduction of high frequency noise, the signals are smoothed by the median algorithm of the software[1]. Then raw data is further processed by Matlab software for accessing the image files. The 'Get Data Graph Digitizer' software is used to obtain the amplitude perturbations and the observed peak time.

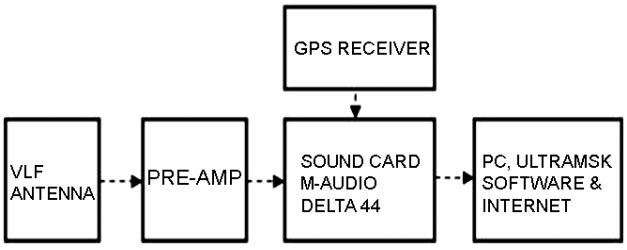

Fig. 1 — Block diagram of the VLF receiver

Figure 2 shows the location of VLF receiver at TNU, the NWC transmitter at Australia and great circle path. The TNU-NWC path mainly over the sea is located on the equatorial region. Figure 3 shows the diurnal variation of NWC signal recorded on 25 October 2013 with two clear disturbed amplitudes due to strong solar flares, the mean of solar quite days's signal, and variation of X-ray intensity on 25 October 2013.

Based on the intensity, the solar flares are divided into specific classes for different levels, including B, C, M, and X classes. The B class is the smallest class and the X class is the greatest class. Each class is divided into the levels from 1.0 to 9.9 (Ref. 12). In order to perform an exact analysis, the flare peak time is captured from GOES (Geostationary Operational Environmental Satellite) data via the website http://www.swpc.noaa.gov/ftpmenu/lists/xray.html. In this work, the solar flare events are considered with the zenith angle less than 65° because the observed perturbations are not significantly affected by the zenith angles[10]. These angles are dependent on the latitude and local time.

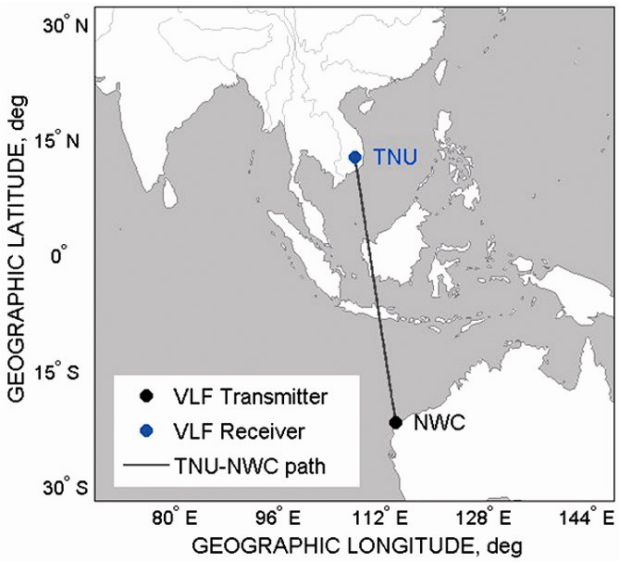

Fig. 2 — Map showing the locations of VLF receiver, NWC transmitter and the TNU-NWC path

The zenith angle is calculated by the website service of http://www.esrl.noaa.gov/gmd/grad/solcalc/azel.html. The amplitude perturbations ΔA (in dB unit) are determined by subtracting the quiet day data[8,15-18] from the VLF receiver data:

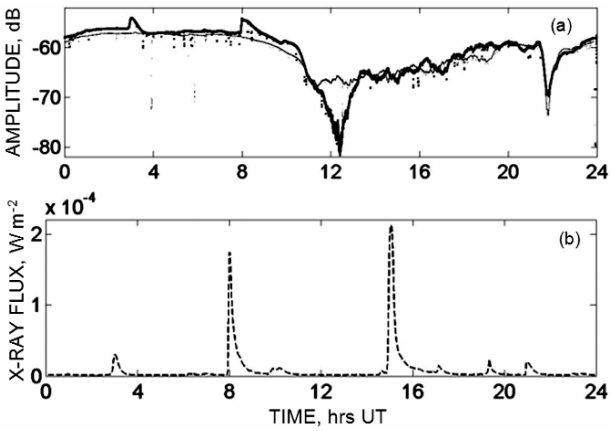

Fig. 3 — (a) Diurnal variation of NWC signal and perturbation amplitudes *versus* time on 25 Oct 2013: (thick solid line) due to solar flares; (thin solid line) quiet VLF amplitude [mean of four quiet days' data]; (b) Variation of solar X-ray flux *versus* time on 25 Oct 2013 with solar flares of different classes, M2.99 at 03:02 hrs UT, X1.7 at 08:01 hrs UT, and M1.08 at 10:12 hrs UT, which enhances the VLF amplitude in daytime

$$\Delta A = A_p - A_q \quad \ldots (2)$$

where, A_p, is maximum VLF perturbation for a given solar flare; and A_q, *the* mean of four available solar-quiet days' data which are closest to the disturbed days. The solar quiet days include the days, which are not significantly affected by the tiny solar flares[13].

These perturbations ΔA are added to the simulated unperturbed amplitude (A_{lwpc}) that is obtained from the LWPC default program at the receiver site to obtain:

$$A_p^{'} = A_{lwpc} + \Delta A \quad \ldots (3)$$

These input parameters of A'_p are used for obtaining the H' and β under perturbed ionosphere conditions. These results are used in Eq. (1) to calculate the electron density, N_e. Using the LWPC program[19] for TNU-NWC path, the unperturbed amplitude of 66.494 dB is obtained, which corresponds to H' = 74.0 km, $\beta = 0.3$ km^{-1} and N_e = 2.18E+08 m^{-3}.

3 Results

About 26 solar flare events were recorded from C2.56 to X3.2 classes. Table 1 shows the data related to the observed solar flare events which are chosen

Table 1—Datasheet of all observed solar flares

Date	Flare class	I_X, Wm^{-2}	ΔA, dB	FPT, hrs UT	OPT, hrs UT	χ, deg	H', km	β, km^{-1}	N_e at 74 km, m^{-3}
05 May	C8.0	8.00E-06	1.4397	0:49	0:52	56	62.2	0.327	1.024E+10
14 May	X3.2	3.20E-04	3.9965	1:11	1:08	52	60.0	0.506	2.578E+11
15 May	X1.2	1.20E-04	3.3382	1:48	1:43	44	60.0	0.434	9.407E+10
28 Jun	C4.4	4.40E-06	0.6250	1:59	1:58	42	71.0	0.315	5.560E+08
28 Jun	C7.3	7.30E-06	0.5536	3:37	3:41	20	70.5	0.308	6.351E+08
15 Oct	C9.52	9.52E-06	2.4214	5:07	5:09	23	60.3	0.372	3.532E+10
22 Oct	C4.0	4.08E-06	0.5429	4:21	4:23	24	70.1	0.303	7.045E+08
24 Oct	C9.4	9.40E-06	1.3071	5:59	6:01	33	63.3	0.320	6.633E+09
25 Oct	M2.99	2.99E-05	3.1489	3:02	3:01	34	60.0	0.434	9.407E+10
25 Oct	X1.74	1.74E-04	3.8434	8:01	8:00	57	60.3	0.485	1.661E+11
26 Oct	M2.33	2.33E-05	3.1000	6:06	6:08	35	60.1	0.414	6.821E+10
27 Oct	C4.31	4.31E-06	1.1714	3:30	3:34	29	63.4	0.315	6.092E+09
03 Nov	M4.96	4.96E-05	2.2929	5:22	5:23	31	61.1	0.365	2.396E+10
05 Nov	M2.5	2.50E-05	1.3830	8:18	8:20	63	62.8	0.324	8.140E+09
06 Nov	M1.8	1.80E-05	2.7714	8:38	8:39	65	60.3	0.392	4.645E+10
07 Nov	C4.32	4.32E-06	1.2500	8:23	8:25	65	63.3	0.318	6.492E+09
13 Nov	C2.68	2.68E-06	0.9078	4:42	4:46	31	64.4	0.304	4.000E+09
13 Nov	C6.59	6.59E-06	1.2199	3:58	4:01	32	63.3	0.317	6.423E+09
15 Nov	M1.08	1.08E-05	1.3333	2:29	2:31	43	62.9	0.322	7.708E+09
16 Nov	C2.56	2.56E-06	0.5714	2:05	2:08	48	69.7	0.301	7.885E+08
16 Nov	M1.67	1.67E-05	1.3214	7:49	7:52	58	63.1	0.321	7.149E+09
23 Nov	M1.18	1.18E-05	1.8214	2:32	2:35	44	61.9	0.343	1.371E+10
04 Dec	C4.75	4.75E-06	0.5000	4:58	4:58	35	71.3	0.310	4.991E+08
07 Dec	M1.27	1.27E-05	0.9714	7:29	7:28	54	64.0	0.307	4.655E+09
25 Dec	C4.73	4.73E-06	0.5409	6:39	6:43	46	70.1	0.303	7.045E+08
29 Dec	M3.17	3.17E-05	2.0571	7:56	7:58	58	61.9	0.353	1.548E+10

with the zenith angles less than 65°. The zenith angles for the receiver site are 12.56°N, 108.02°E.

The data was analyzed and the LWPC program was used to calculate Wait's parameters. It was found that as the X-ray intensity increased, the H' fell down from 74 to 60 km and β increased from 0.30 to 0.506 km^{-1}. The electron density at the height of 74 km increased about 1-3 orders of magnitude. At C2.56 class flare event on 16 November 2013, the electron density increased to 7.885E +08 m^{-3} and the highest class, X3.2, increased on 14 May 2013 to 2.578E +11 m^{-3}. Most of the amplitude peaks occurred about 1 – 4 min after the X-ray flare flux peaks (I_X). These time delays needed for the D-region recombination – ionization processes to recover balance under the enhancement of X-ray irradiance[15].

Two solar flare events of 25 October and 07 November, 2013 are presented in Fig. 4 and Table 2. The X-ray intensity of M2.99 and C4.32 class was maximum at 03:02 and 08:23 hrs UT, respectively. The recorded peak signal amplitude was maximum at 03:01 and 08:26 hrs UT, and the VLF amplitudes increased to about 3.0744 dB and 1.2423 dB, respectively. At the pre-flare state, the amplitudes of VLF signals are higher than those at the quiet condition. After about 40 minutes, the disturbed amplitudes returned to normal levels. For the solar flare event on 07 November, the VLF signal amplitude peak appeared about 3 minutes after the peak of X-ray flux. Conversely, in the solar event on 25 October, the VLF signal amplitude peak occurred about 1 minute before the X-ray flare peak.

The perturbed amplitude and time delay presented in Table 1 are also plotted as functions of corresponding peak flare flux in Figs 5(a and b). It is found that positive amplitude perturbation has gone up to 4 dB for X3.2 class flare and time delay has a tendency of decreasing with enhancement of X-ray intensity. The time delay varied 35 – 242 s.

Table 2 shows parameters H', β and electron densities, Ne, at different times during solar flares. In the column 3 and 4, the flare peak times (FPT) and the observed peak time (OPT), respectively are presented. In column 5, the time before flare peak region, at the maximum value of VLF amplitude and

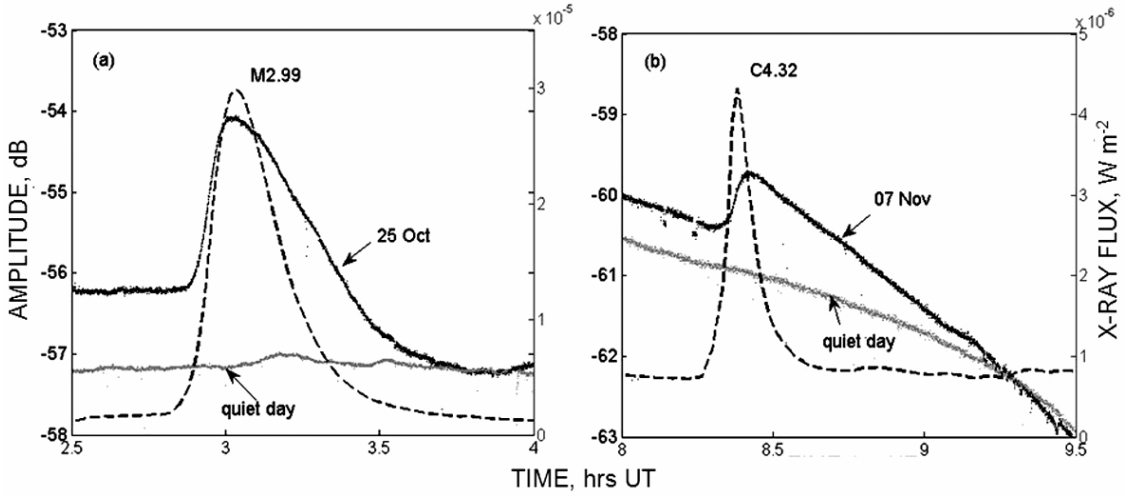

Fig. 4 — Time variation of X–ray irradiance of: (a) M2.99; and (b) C4.32 events (dashed line) with the peaks at 03:02 hrs UT on 25 October and at 08:23 hrs UT on 07 November 2013; the corresponding disturbances of NWC signal amplitude (thick solid line) with the peak at 03:01 hrs UT and 08:26 hrs UT, respectively [mean of four quiet days' data is shown by the light blue line]

Table 2—Example of the ionospheric parameter changes during solar flares

Date	Flare class	FPT, hrs UT	OPT, hrs UT	Time, hrs UT	ΔA, dB	H', km	β, km^{-1}	N_e, m^{-3}
25 Oct	M2.99	3:02	3:01	2:44	0.9709	65.2	0.304	3.137E+09
				3:01	3.0744	60.0	0.434	9.407E+10
				3:40	0.0971	71.4	0.305	4.776E+08
07 Nov	C4.32	8:23	8:26	8:16	0.4755	73.1	0.317	2.875E+08
				8:26	1.2423	63.3	0.318	6.492E+09
				9:11	0.1534	73.8	0.306	2.297E+08

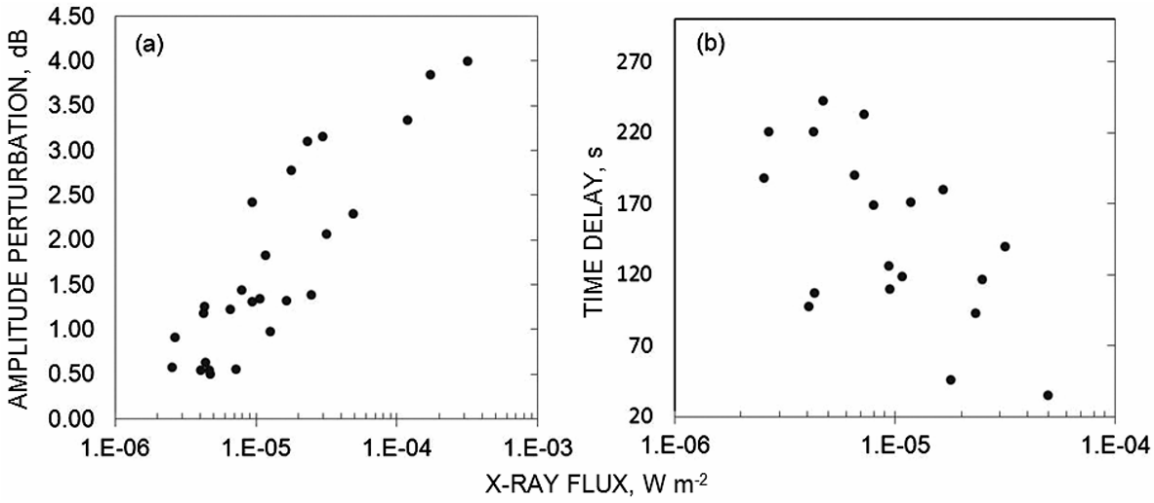

Fig. 5 — (a) Perturbed amplitude versus maximum X-ray flux for all 26 flares; (b) Time delay versus maximum X-ray flux for solar flare events which X-ray flux peaks occurred before the VLF amplitude peaks

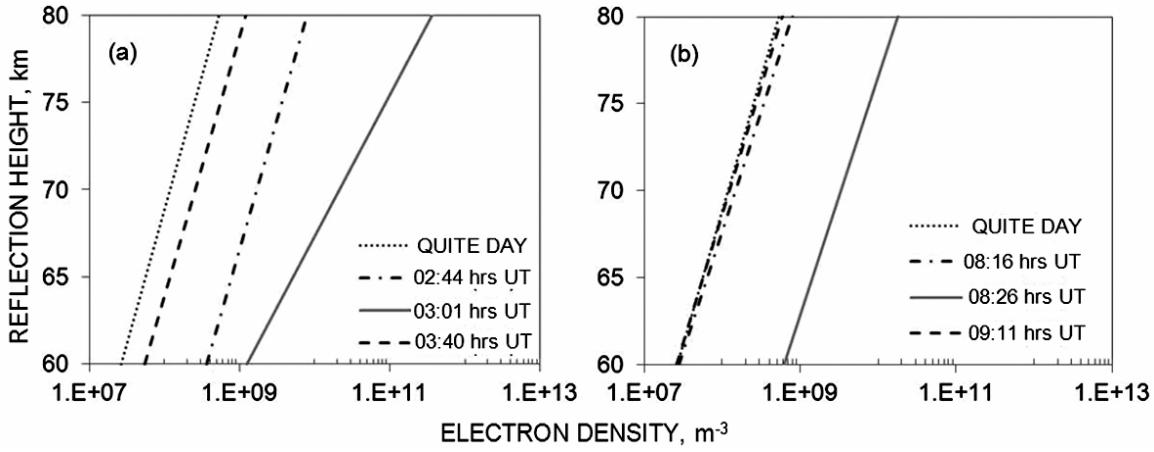

Fig. 6 — Changes in the electron density profile from 60 to 80 km during: (a) M2.99 X-ray flare event on 25 October 2013; (b) C4.32 X-ray flare event on 07 November 2013 [electron number density's axis is shown the logarithmic scale with base 10]

after the flare region is shown. The electron density is calculated by Eq. (1) at the height of 74 km.

In Fig. 6, the changes of electron density with the height for the M2.99 and C4.32 flare events are presented. The electron profiles of quiet day (H' = 74 km, β = 0.3 km), before flare peak region, at the flare peak region and after the flare region are also plotted by dotted, dot-dashed, solid and dashed lines, respectively.

The LWPC program is used to calculate the electron density (N_e) at the height of 74 km. This electron density (N_e) and the perturbation amplitude (A_p) of two solar events are plotted and shown in Fig. 7. It is observed that the shape of electron density variation nearly follows the NWC signal amplitude. Figure 8 shows the 3D plot of electron density variation during solar flare with the height, from 60 to 80 km, for the sufficient view.

4 Discussion

Almost peaks of perturbed VLF amplitude occurred before the X-ray flux peaks. However, in some cases, VLF amplitude peaks appeared prior to the corresponding X-ray flux peaks. These events mostly occurred for strong class flares. The occurrences of X3.2 class flare on 14 May and X1.2 class flare on 15 May started near the sunrise. The effects of these events are not very apparent because the day/night changes of propagation medium are more severe than effects of solar flare event for the strongest flares[20]. Before M2.99 and X1.74 class flares on 25 October, there is a series of C class flares,

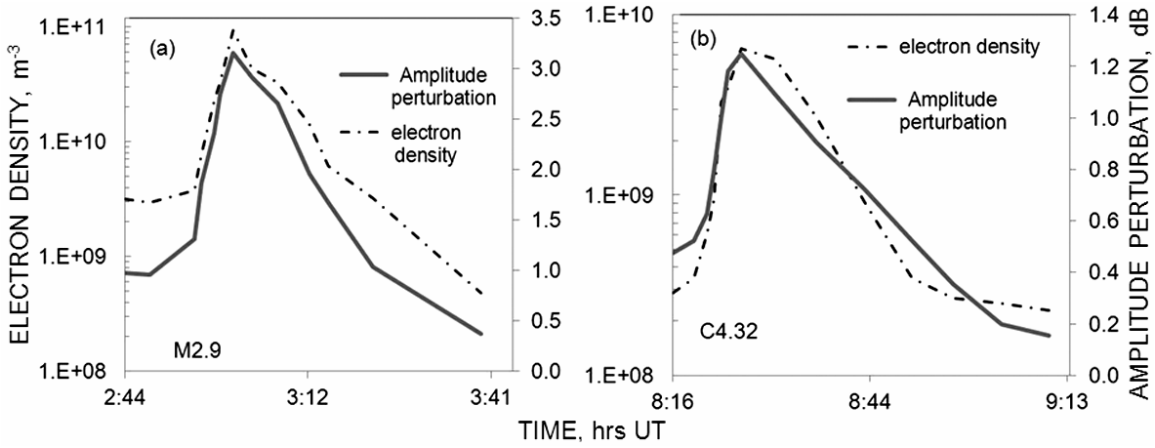

Fig. 7 — 2D picture showing comparison of the shape of the temporal variations of electron density at 74 km height and the amplitude perturbations of NWC signal due to: (a) M2.99 class solar flares events; (b) C4.32 class solar flare events

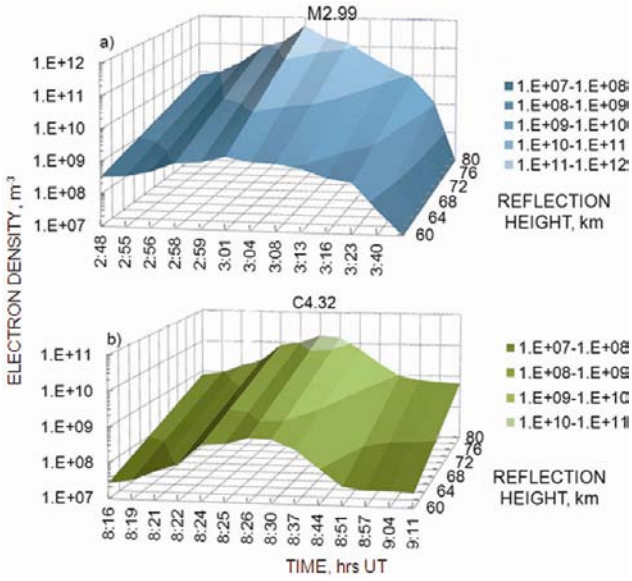

Fig. 8 — 3D picture showing the shape of the variations of electron density with the height from 60 to 80 km and time of: (a) M2.99 class flare events; (b) C4.32 class flare events

which initially increase the ionization rate. Hence, the amplitude remained more than the regular level in quite days before the onset of next flare. After that, the later solar flares cause the extra ionization[21]. When strong solar flare occurred after a series of C class flares, the X-ray strength in pre-flare is strong enough to make the saturation of the increase of electron density, and then the VLF amplitude peaks are produced before the X-ray peaks.

In Fig. 6, when the peak of VLF amplitude occurred, the variation of the electron density profiles of both flare events became steeper and the sharpness factors β reached the highest values. At the lower altitudes, i.e. about 60 km, the electron density increased to 1 - 2 orders of magnitude for M2.99 and C4.32 flare classes; while at the higher altitudes, i.e. about 80 km, the electron density increased to 1 - 3 orders of magnitude for M2.99 flare class; and 1 - 2 orders of magnitude for C4.32 flare class. In the recovery phase (the amplitude of VLF signal returned to the unperturbed level of amplitude), the electron number density distribution went back to its normal value in the undisturbed condition. It was also observed that the returned normal level process of the C class flare events was faster than that of the M class flare events. However, in this state, the value β was still not equal to its normal value. Figure 7 shows that the shape variation of N_e is roughly similar to that of the amplitude perturbation. These results are in conformity with the results of Basak & Chakrabarti[13] and Zigman *et al.*[15]. In Fig. 8, it is interesting that the variation of electron density with the height keeps the same shape. The variation of the zonal colour which looks like the "V" letter, corresponding to the variation of electron height density, seems to be symmetrically expanded on the curved surface.

According to the observed results of Grubor *et al.*[8], from C to M5 classes during the summer months of 2004 – 2007, in Belgrade, Serbia (44.85°N, 20.38°E), the electron density at a height of 74 km is 2.16E+8 m^{-3} in the undisturbed conditions and it is 40E+9 m^{-3} in the turbulence condition (M5 flare class). The β increased from 0.3 to 0.49 km^{-1} and *H'* reduced from 74 to 63 km (Ref. 8). Basak & Chakrabarti[13] analyzed 22 events of flare from C1.5 to M9.31 classes during January - September 2011 in Sitapur, India (22.45°N, 87.75°E) with zenith angles 15° - 30°.

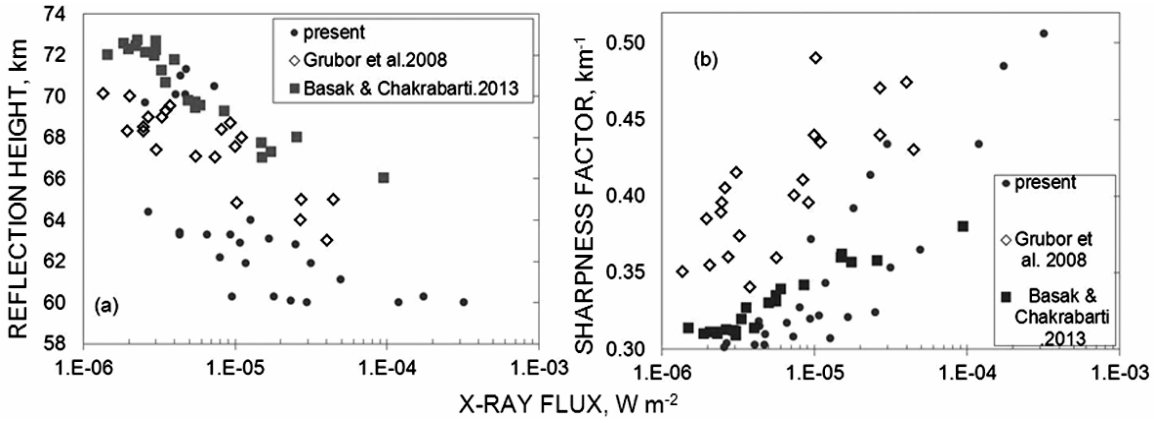

Fig. 9 — (a) Reflection height, H', versus X-ray irradiance; (b) Ionospheric sharpness factor, β, versus X-ray irradiance

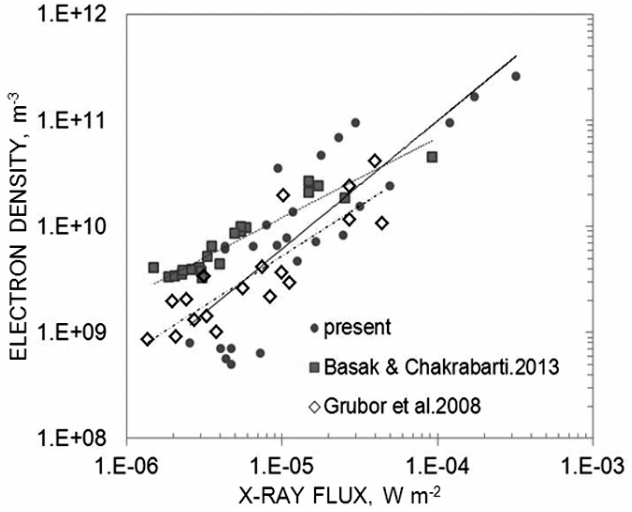

Fig. 10 — Electron density at 74 km versus X-ray intensity of: (circles) C2.56 - X3.2 flare classes observed at Tay Nguyen University; (squares) C1.5 - M9.31 flare classes which Basak & Chakrabarti observed at receiver in Sitapur, India (22.45°N, 87.75°E); (diamonds) C - M5 flare classes which Grubor observed at the receiver in Belgrade, Serbia (44.85°N, 20.38°E)

In Fig. 9, it is shown that the parameters β, in Basak & Chakrabarti's[13] results, at the same series of flare are lower than that Grubor *et al*'s.[8] results, but the parameters *H'* in Basak & Chakrabarti's[13] results are higher than that of present results and Grubor *et al.*'s [8] results. The changes of the two parameters versus the X-ray intensity observed in the present study are thoroughly in agreement with the rules found by Basak & Chakrabarti[13] and Grubor *et al.*[8]. From Fig. 9(b), it can be concluded that the TNU-NWC path with the length of 3886 km, which is the long path, changes of VLF signal amplitude strongly depend on the sharpness factor, β. This is in consistent with the results of Thomson[12]. However, in the series flare from C to M classes of present results, it can be preliminarily concluded that the reflection height, *H'*, decreases faster than that found in the results of Basak & Chakrabarti[13] and Gubor *et al.*[8], whereas the changes of the sharpness factor, β, are consistent with Basak & Chakrabarti's[13] results and its values are lower than what observed in Grubor *et al.*'s[8] results. The obtained Wait's parameters of the present work are significantly dispersed due to the effects of seasonal factors.

In Fig. 10, it is found that the electron density, in present our results, increases more rapidly with the altitude (the slope of the fitted line has the highest value) than what had been observed in the results of Basak & Chakrabarti[13], and Grubor et al.[8] The enhancements of the electron density during solar flares can be explained as: the ionization due to X-ray irradiance at altitudes of D-region becomes greater than what occurs due to cosmic rays and Lyman-α radiation, which increases the electron density profile[10]. In addition, the electron density observed by the receiver with the TNU-NWC path mainly over the equatorial region increases more rapidly due to the effects of the equatorial ionization anomaly region[23,24]. The effects of solar X-ray irradiance on the upper VLF waveguide boundary cause the descending of the lower edge of the ionosphere because of electron density increase[16]. Therefore, the reflection height in the present work is lower than that of the results of other researchers.

5 Conclusions

In the present study, 26 solar flare events from C2.56 to X3.2 at Tay Nguyen University were recorded and analyzed during May – December 2013. It is concluded that:

- When the X-ray intensity increased, the β increased from 0.3 to 0.506 km^{-1}, while H' decreased from 74 to 60 km.
- The 3D representation of the electron density changes with altitude and time supports to clearly understand the shape of the electron density changes during solar flares.
- The shape variation of N_e roughly followed the variation of the amplitude perturbation. The returned normal level process of the C class flare events was faster than that of the M class flare events, but after the flare region, the value of β was still not same as its normal value.
- The electron density of lower latitude D-region ionosphere during solar flares increases more rapidly.

The present work contributes to understand the responses of lower ionosphere due to solar flares at low latitude. In future, the work is likely to be continued to study the characteristics of the low-latitude D-region ionosphere using the VLF amplitude observation and its time delay during solar flares.

Acknowledgement

The authors would like to thank James Brundell for guiding the use of UltraMSK software. They also acknowledge the X-ray data provided by the US National Geophysical Data Center.

References

1 Gustafsson M, *Detection of solar flare induced ionospheric perturbations on narrowband VLF transmissions*, MS Thesis, KTH School of Electrical Engineering, Stockholm, Sweden, 2011.

2 Hunsucker R D & Hargreaves J K, *The high-latitude ionosphere and its effects on radio propagation* (Cambridge University Press, UK), 2003, 617.

3 Scherrer D, Mitchell R, Huynh T, Lord W & Lord M, *Super SID manual – Space weather monitor* (Stanford Solar Center, USA), 2009.

4 Merola L A, *A study of the effects of Sunrise and Sunset on the Ionosphere* (South Side High School, USA), 2008.

5 Davies K, *Ionospheric radio propagation* (US Government Printing Office, Washington, DC), 1965, 470.

6 More C T, Sharma A K, Bhonsle R V & Lynn Kenneth J W, *Field strength measurement of VLF radio wave propagation at 19.8 kHz between Australia and India*, Proceeding of the 10th Australia Space Science Conference, Brisbane, Australia, 27 – 30 Sept 2010 (National Space Society of Australia, Australia), 2010.

7 Lynn K J W, VLF waveguide propagation: The basics, *AIP Conf Proc (USA)*, 1286 (2010) 3, doi: 10.1063/1.3512893.

8 Grubor D, Šulíc D & Žigman V, Classification of X-ray solar flares regarding their effects on the lower ionosphere electron density profile, *Ann Geophys (Germany)*, 26 (2008) 1731.

9 Mitra A P, *Ionospheric effects of solar flares* (D Reidel, Holland), 1974, 294.

10 Thomson N R & Clilverd M A, Solar flare induced ionospheric D-region enhancements from VLF amplitude observations, *J Atmos Sol-Terr Phys (UK)*, 63 (2001) pp 1729-1737.

11 Wait J R, *Electromagnetic waves in stratified media* (Pergamon, New York), 1962, 372

12 Thomson N R, Experimental daytime VLF ionospheric parameters, *J Atmos Terr Phys (UK)*, 55 (1993) pp 173-184.

13 Basak T & Chakrabarti S K, Effective recombination coefficient and solar zenith angle effects on low-latitude D-region ionosphere evaluated from VLF signal amplitude and its time delay during X-ray solar flares, *Astrophys Space Sci (Netherlands)*, 348 (2013) 315.

14 Dahlgren H, Sundberg T, Andrew B C, Koen E & Meyer S, Solar flares detected by the new narrow band VLF receiver at SANAE IV, *South African J Sci (South Africa)*, 107 (2011) 9.

15 Žigman V, Grubor D & Šulíc D, D-region electron density evaluated from VLF amplitude time delay during X-ray solar flares, *J Atmos Sol-Terr Phys (UK)*, 69 (2007) pp 775-792.

16 Kolarski A & Grubor D, Sensing the Earth's low ionosphere during solar flares using VLF signals and Goes Solar X-Ray data, *Adv Space Res (UK)*, 2014, doi: http://dx.doi.org/10.1016/j.asr.2014.02.022.

17 Palit S, Basak T, Mondal S K, Pal S & Chakrabarti S K, Modeling of very low frequency (VLF) radio wave signal profile due to solar flares using the GEANT4 Monte Carlo simulation coupled with ionosperic chemistry, *Atmos Chem Phys (Germany)*, 13 (2013) 9159.

18 Pal S & Chakrabarti S K, Theoretical models for computing VLF wave amplitude and phase and their applications, *AIP Conf Proc (USA)*, 1286 (2010) 42.

19 Ferguson J A, *Computer programs for assessment of long-wavelength radio communications, version 2.0* (Space and Naval Warfare Systems Center, San Diego, CA), 1998.

20 Grubor D, Šulíc D & Žigman V, Influence of solar X-ray flares on the Earth-Ionosphere waveguide, *Serb Astron J (Serbia)*, 171 (2005) 29.

21 Kuma A, *Amplitude and phase study of sub-ionospheric VLF radio signal receiver at Suva*, MS Thesis, The University of the South Pacific, Suva, Fiji, 2007.

22 Basak T, Pal S & Chakrabarti S K, *VLF study of ionospheric properties during solar flares of varied intensity for a fixed propagation path*, Paper presented to General Assembly and Scientific Symposium, XXXth URSI, Istanbul, Turkey, 2011.

23 Zhao B, Wan W, Liu L & Ren Z, Characteristics of the ionospheric total electron content of the equatorial ionization anomaly in the Asian-Australian region during 1996–2004, *Ann Geophys (Germany)*, 27 (2009) 3861.

24 Bhattacharya S, Purohit P K & Gwal A K, Ionospheric time delay variations in the equatorial anomaly region during low solar activity using GPS, *Indian J Radio Space Phys*, 38 (2009) 266.